Thermal Design of the CAESAR Multi-Degree-of-Freedom Robotic Arm for On-Orbit Servicing

Ralph Bayer[1] and Alexander Beyer[2]
German Aerospace Center (DLR e.V.), Weßling, Bavaria, 82234, Germany

Markus Czupalla[3]
FH Aachen – University of Applied Sciences Aachen, Aachen, North Rhine-Westphalia, 52064, Germany

Manfred Schedl[2] and Maximo A. Roa[2]
German Aerospace Center (DLR e.V.), Weßling, Bavaria, 82234, Germany

The Compliant Assistance and Exploration SpAce Robot (CAESAR) is a seven-degree-of-freedom robotic arm developed at the Institute of Robotics and Mechatronics (RM) of the German Aerospace Center (DLR) as a servicing asset for missions in LEO, GEO and beyond. CAESAR's upcoming flight application is the European Robotic Orbital Support Services - Servicing Component (EROSS SC) on-orbit servicing mission, whose demanding LEO environment and operational scenarios drive the arm's thermal requirements. This paper presents the thermal architecture and modeling approach for CAESAR, building on its multi-orbit servicing design and adapting it into mission-ready hardware for EROSS SC. The thermal design combines multi-layer insulation, radiators and distributed heaters to control temperatures and gradients in joints, electronics and structure. The arm must remain functional across a broad Sun-synchronous orbit (SSO) envelope, with varying altitudes and environmental conditions, as well as servicer attitudes and arm configurations, while performing close-range capture and manipulation of an unprepared or prepared client satellite and Orbital Replacement Unit (ORU) transfer operations. The combination of seven robotic joints and varying illumination conditions creates a multidimensional configuration space that challenges traditional sizing approaches based on limited analysis cases. To address this, a kinematically configurable ESATAN-TMS model of the arm has been developed and applied to initial chasing-mode orbital cases with selected arm postures. These cases are used to size heater zones, assess margins to temperature limits, and identify gradients along the arm. The paper summarizes the modeling approach, worst-case environments and design trades for chasing operations, including radiator self-viewing and arm–servicer heat exchange, and shows its applicability to future articulated servicing arms. The segment-level results indicate compliance for the assessed cases, with self-shadowing configurations being particularly sensitive due to reduced heat rejection. Future work will address proximity operations and coupled thermal interactions between the servicer and the client satellite.

Acronyms and Nomenclature

α	=	Solar absorptivity
ε	=	Infrared emissivity
AA	=	Aluminium Alloy
AIT	=	Assembly, Integration and Test
CAESAR	=	Compliant Assistance and Exploration Space Robot
DLR	=	Deutsches Zentrum für Luft- und Raumfahrt (German Aerospace Center)
DoF	=	Degree of Freedom
EB	=	Electronic Block

[1] Researcher, Institute of Robotics and Mechatronics, Münchener Strasse 20, 82234 Weßling, Germany, Ralph.Bayer@dlr.de
[2] Researcher, Institute of Robotics and Mechatronics, Münchener Strasse 20, 82234 Weßling, Germany
[3] Professor, FH Aachen – Aerospace and Automotive Engineering, Hohenstaufenallee 6, 52064 Aachen, Germany

EMC	=	Electromagnetic Compatibility
ERA	=	European Robotic Arm
EROSS SC	=	European Robotic Orbital Support Services - Servicing Component
HaDEA	=	European Health and Digital Executive Agency
HL	=	Heating Line
ISS	=	International Space Station
LAR	=	Launch Adapter Ring
LARIS	=	Launch Adapter Ring Interface System
MLI	=	Multi-Layer Insulation
NTC	=	Negative Temperature Coefficient
ORU	=	Orbital Replacement Unit
OOS	=	On-Orbit servicing
PCB	=	Printed Circuit Board
PIAPS	=	PIAP Space
RAAN	=	Right Ascension of the Ascending Node
RAVS	=	Robotic Assembly Vision System
RAS	=	Robotic Assembly System
RM	=	Institute of Robotics and Mechatronics
ROKVISS	=	Robotics Component Verification on ISS
SpaceApps	=	Space Applications Services
SRMS	=	Shuttle Remote Manipulator System
SSM	=	Second-Surface Mirror
SSRMS	=	Space Station Remote Manipulator System
SSO	=	Sun-Synchronous Orbit
TASF	=	Thales Alenia Space France
TBT	=	Thermal Balance Test
TCS	=	Temperature Control System
TCP	=	Temperature Control Point
TVAC	=	Thermal Vacuum Chamber

I. Introduction

On-orbit servicing (OOS) is progressing from a long-standing concept toward mission-ready architectures and flight hardware. Representative objectives include satellite inspection, repair, life extension, and end-of-life disposal, complemented by functions such as refuelling, orbit maintenance and correction, hardware replacement or upgrade, in-orbit assembly, and debris removal.

For OOS architectures that go beyond docking-based life extension, articulated multi-degree-of-freedom (multi-DoF) robotic arms become a key driver of the overall system design. They provide close-range physical interactions with the target satellite, from capture and secure mechanical attachment to in-situ servicing operations (e.g., inspection support, Orbital Replacement Unit (ORU) exchange, or tool-based interventions). Robotic arms also draw on extensive on-orbit heritage, from the Shuttle Remote Manipulator System (SRMS/Canadarm) on the Space Shuttle [1] to International Space Station (ISS) systems such as the Space Station Remote Manipulator System (SSRMS/Canadarm2) [2] and ESA's European Robotic Arm (ERA) [3], providing a well-established reference for free-flying servicing missions.

Such an articulated multi-DoF robotic system is the Compliant Assistance and Exploration SpAce Robot (CAESAR), a robotic arm for OOS missions developed at the German Aerospace Center (DLR), Institute of Robotics and Mechatronics (RM) [4]. CAESAR's mechatronic design is tailored to the associated requirements and constraints and builds on RM's space robotics heritage, including the Robotics Component Verification on ISS (ROKVISS) in-orbit experiment [5].

From a thermal perspective, the required robustness of the robotic system is shaped by multiple factors across the mission envelope, and the complexity increases when the servicing concept aims to be compatible with multiple target satellites in different orbital conditions.

A major source of variability is the orbital thermal environment, particularly in LEO, where time-varying external fluxes can lead to strong cyclic changes in radiative loads as the satellite transitions between sunlit and eclipse conditions. Additionally, robotic-arm kinematics lead to configuration-dependent thermal boundary conditions through changing self-shadowing and radiative view factors. During close-proximity operations, mutual radiative coupling and shadowing between the servicer, robot, and target depend on their relative geometry and the thermo-optical properties of the interacting surfaces.

CAESAR's next planned flight application is EROSS SC (European Robotic Orbital Support Services – Servicing Component). The mission covers rendezvous of a servicer with a cooperative client satellite, followed by capture and servicing operations. As a European demonstration mission, it is intended to validate the feasibility of such end-to-end on-orbit servicing operations for future missions [6].

This paper presents the thermal design of the CAESAR robotic arm for the EROSS SC servicing context. A mission-relevant ESATAN-TMS case study is defined using representative orbital environments and arm configurations, and first analysis results quantify temperature margins and heater power demand.

II. EROSS SC Mission Overview

EROSS SC is the latest phase of the EROSS programme, an in-orbit technology demonstration project funded by the European Union. Coordinated by Thales Alenia Space France (TASF), a consortium of 17 partners develops, integrates, and validates key technologies for autonomous robotic OOS for a LEO demonstration mission that defines an end-to-end servicing chain, with a servicer satellite interacting with a cooperative client satellite [7].

The mission scope includes rendezvous and inspection, close-range operations such as docking and station keeping, and servicing-relevant tasks including ORU transfer and refuelling. It further distinguishes between prepared and unprepared client conditions, for example via capture using a launch adapter ring feature versus a dedicated grasping fixture, to cover representative interface cases.

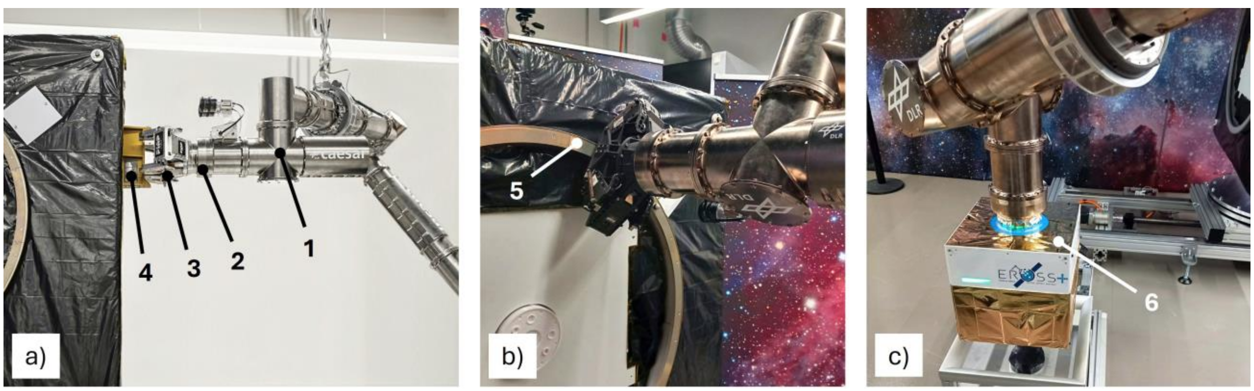

Figure 1. Representative RAS demonstrations: a) capture of a prepared client mock-up via the SGF interface (4) using the CAESAR arm (1) equipped with HOTDOCK (2) and LARIS gripper (3), b) capture of an unprepared client mock-up via the LAR (5), c) ORU mock-up (6) manipulation.

The demonstrator scenario foresees a servicer and a dummy client co-launched into a LEO orbit and separated after launcher injection. The two satellites are subsequently operated independently until the servicer performs approach and initiates capture and servicing demonstrations, followed by deorbiting of the dummy client using the servicer propulsion at end of mission [8].

A core element of EROSS SC is the robotic assembly system (RAS), which includes several subsystems for capture and servicing tasks and therefore enables physical interaction with the client. Representative RAS demonstrations are shown in Figure 1.

CAESAR, developed by DLR RM, provides the articulated manipulation capability and supports position- and torque-controlled operation through joint torque sensing and impedance-based control.

HOTDOCK, developed by Space Application Services (SpaceApps), is the standardized docking interface of the RAS and provides the mechanical, electrical, and data interfaces for coupling exchangeable end effectors and ORUs. The active side is integrated at the CAESAR arm tip and mates with passive counterparts on a capture tool and ORUs, enabling direct handling and transfer operations [9].

The Launch Adapter Ring Interface System (LARIS) gripper, developed by PIAP Space (PIAPS), serves as the dedicated end-effector tool and supports capture in both unprepared and prepared client interface cases, for example by grasping a launch adapter ring (LAR) or the dedicated Standard Grasping Fixture (SGF) [10].

III. Thermal Environment

Within the EROSS SC mission context, the CAESAR thermal design is driven by the cyclic LEO environment. Periodic eclipse transitions and Earth-view-dependent contributions of direct solar, Earth infrared and Earth-reflected (albedo) flux lead to pronounced variations of the external thermal boundary conditions along the orbit. Table 1 summarizes the external environment parameters assumed for the thermal design reference cases and sensitivity coverage.

Table 1. Thermal Environment Parameter.

Condition	Solar Flux	Earth Flux	Albedo	Inclination	Alttitude	RAAN	Sun Declination
Hot	1414 W/m²	267 W/m²	0.35	97.5°	525 km	0°-90°	±23.4°
Cold	1322 W/m²	214 W/m²	0.25				

The demonstration mission foresees a Sun-synchronous orbit (SSO), which is typically characterized by an inclination in the range of 97° to 98°. For the thermal design verification, a mean value is adopted.

While the servicer's operational altitude is expected to vary over the mission, a representative reference altitude of 525 km is selected to define the baseline environment for this phase.

To support robust thermal sizing of CAESAR without over-constraining future on-orbit operations, the orbit-to-Sun geometry is covered over a deliberately broad range of right ascension of the ascending node (RAAN) and Sun declination. This captures the associated Earth-eclipse conditions and the variation in solar incidence that drives orientation-dependent shadowing in both operational and non-operational cases.

Alongside the orbit-to-Sun geometry coverage, the external radiative environment is represented by conservative hot and cold cases for direct solar irradiance, Earth infrared flux, and albedo.

IV. CAESAR Arm

CAESAR follows a building-block architecture in which standardized joint modules are combined with structural links to realize different kinematic layouts. This approach allows the workspace to be tailored to operational tasks through the number of joints and link lengths, while maintaining a common mechatronic and control concept.

In the EROSS SC mission context, a seven-DoF arm kinematic layout with a length of about 3 m has been selected to provide the dexterity required for capture and servicing activities (see Figure 2). It supports six-dimensional end-effector tasks and enables self-motion in the null space while preserving the required tool pose. In practice, the tool position and orientation can be maintained while the arm adjusts its joint angles, allowing joint-limit avoidance and the selection of favorable postures in constrained workspaces (e.g., for obstacle avoidance or thermally favorable configurations).

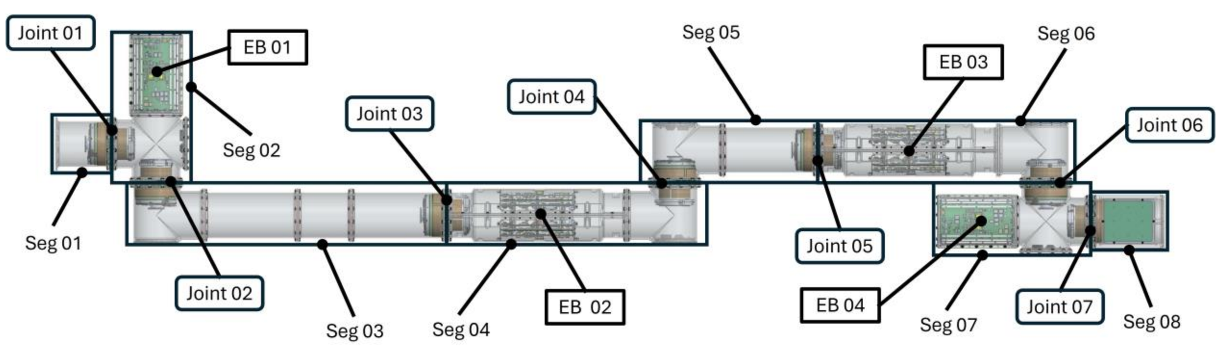

Figure 2. CAESAR arm in the extended (long) configuration with annotated joints, segments, and EBs.

In addition to the joint concept, the electronics also follow a modular architecture. Four Electronic Blocks (EBs) are distributed along the arm. Two EB variants are used: a long and a short version. The long EB is integrated into the arm's structural link, whereas the short EB is side-mounted to the arm. Both versions use an identical set of printed circuit boards (PCBs).

The arm is further partitioned into eight segments, with boundaries defined at joint interfaces. Two segment pairs share the same design (Segments 02 and 07, and Segments 04 and 06), thereby reducing hardware variety, enabling reuse across the mechanical, electrical and thermal architecture, and simplifying assembly, integration and test (AIT).

At the two ends of the kinematic chain, Segment 01 and Segment 08 provide the primary interfaces to the servicer and the end-effector equipment, respectively. Segment 01 forms the base of the arm and provides the mechanical and electrical interface to the servicer. At the end-effector end, Segment 08 accommodates the tool-change interface and the Robotic Assembly Vision Subsystem (RAVS), along with associated electronics to support close-range visual inspection and supervision.

Overall, the modular architecture of the CAESAR arm has direct implications for the thermal design. Joints and EBs are distributed along the kinematic chain and represent both temperature-sensitive components and heat sources, requiring local thermal control while conductively coupling to the surrounding structural housings.

V. The Thermal Design of the CAESAR Arm

The following subsections describe the detailed thermal design of the CAESAR arm across multiple levels of integration, starting with the joint and EB at modular component level. Subsequently, the segment-level design and cross-segment interfaces are introduced to establish the arm-scale thermal concept for the external environment. Finally, the heating-line architecture is described as part of the active thermal control concept used to maintain temperatures in cold conditions.

A. CAESAR Joint

The joint module is the central mechatronic unit of CAESAR and contains the actuation and transmission elements of the arm. A simplified cross-sectional view is shown in Figure 3.

From a kinematic perspective, each joint can be divided into a motor side and a torque side.

The joint's thermal behaviour is primarily defined by a limited set of dominant conductive heat-transfer paths. On the motor side, the motor unit and the commutation sensor electronics are conductively coupled to the segment structure via the motor flange. On the torque side, heat from the torque- and position sensor electronics is conducted into the torque sensor and subsequently transferred to the segment structure via the torque-side structural interface.

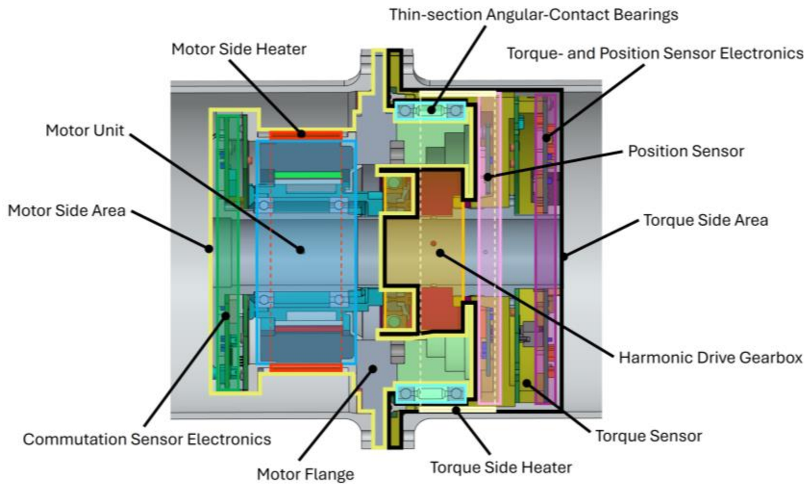

Figure 3. Simplified cross-sectional view of the CAESAR joint.

Both joint sides are mechanically coupled by the drivetrain, which consists of the harmonic-drive gearbox and two preloaded thin-section angular-contact bearings. The assembly transmits torque and motion across the joint and provides the primary conductive thermal link between the joint halves, thereby influencing the temperature distribution along the arm.

Thermally, however, the effective conductance of this link is limited by small contact areas across multiple rotating interfaces within the drivetrain, which leads to high uncertainty in the thermal contact behaviour. The joint was therefore characterized through a dedicated thermal balance test (TBT) campaign, performed in a thermal vacuum chamber (TVAC) under representative boundary conditions.

The resulting measurements, together with the corresponding thermal-model correlation, indicate an effective thermal conductance of ≈ 0.16–0.22 W/K across one thin-section angular-contact bearing interface (inner/outer race contacts), which was identified as the dominant conductive path within the drivetrain. A clear dependence on hot and cold test conditions is observed over the temperature range from +30 °C to −20 °C. The correlated model reproduced the measured temperatures

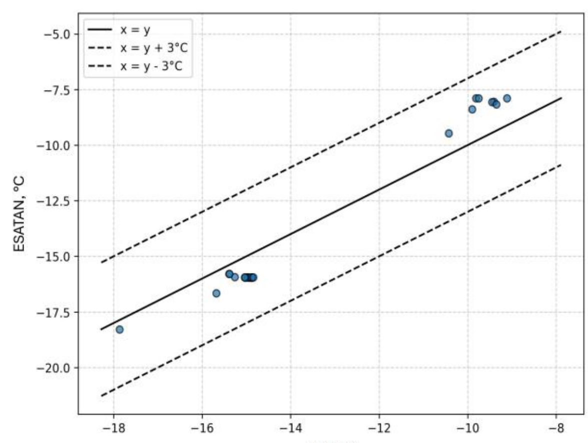

Figure 4. Correlation between measured TBT temperatures and ESATAN-TMS model predictions for the joint in cold case test conditions.

with deviations below ±3 K, providing confidence in the derived conductance range (see Figure 4).

During the test, the joint was kept stationary. As a result, frictional dissipation and lubricant redistribution were absent and did not affect the temperature measurements. A controlled heat flow between the motor and torque sides was applied using dedicated test heater foils on both joint halves.

While the underlying mechanism cannot be isolated from the present data alone, the observed temperature dependence is plausibly attributed to thermo-elastic effects that change the effective preload and thus the thermal contact conditions of the angular-contact bearings.

Several joint subassemblies require controlled temperature levels, including the motor stator and the PCB assemblies located around the joint structure. Of particular relevance is the harmonic-drive gearbox, which is temperature-sensitive due to the Braycote lubricant. Its viscosity increases at low temperatures, leading to higher frictional losses. To support operational supervision of these components, the electronics are equipped with on-board negative temperature coefficient (NTC) thermistors for local temperature monitoring.

Active thermal control is implemented using dedicated heaters to maintain non-operational temperature limits and to preheat the joints into the operational range prior to activation. To mitigate the limited conductive cross-coupling through the drivetrain, heater foils are installed on both joint sides, supporting a more homogeneous temperature field.

Apart from the drivetrain components, which are made of steel, the joint structural and housing parts are predominantly manufactured from aluminium alloy 7075 (AA 7075), providing a comparatively high thermal conductivity and supporting a homogeneous temperature distribution within the joint, where internal heat transfer is dominated by conduction through the structural parts.

Furthermore, the AA 7075 parts are finished with a Surtec 650 coating to ensure electrical conductivity across interfaces and meet electromagnetic compatibility (EMC) requirements. Since the surface finish can exhibit infrared emissivity values as low as $\varepsilon \approx 0.05$, it also influences the thermal behaviour of the joint module by reducing radiative heat exchange internally and with adjacent arm components. However, given the dominant conductive heat transfer, the impact on the temperature distribution is limited.

B. CAESAR Electronic Block (EB)

The EBs contain the joint control and drive electronics and are distributed along the CAESAR arm. From a thermal design perspective, the EBs are treated as individual heat sources with dedicated thermal control concept. A cutaway view of the EB assembly and the main thermal interfaces is shown in Figure 5.

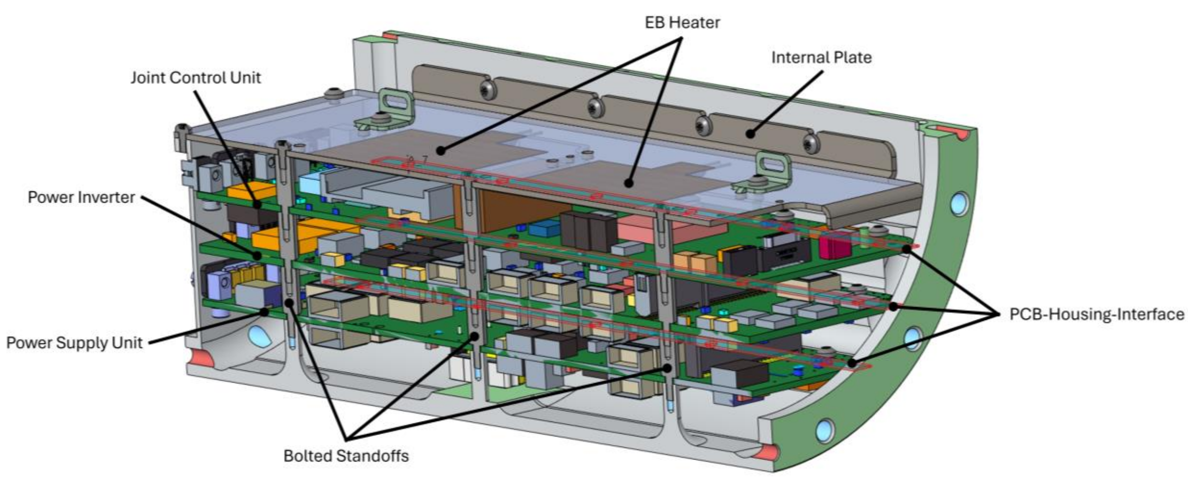

Figure 5. EB half cutaway highlighting the split housing, PCB stack, and key thermal interfaces.

The electronics architecture is cold-redundant, and each EB is divided into a nominal and a redundant half. Mechanically, the EB is realized as a dedicated structural element with a split housing concept, allowing access to the electronics by removing a half shell without splitting the manipulator. Both halves are implemented with an identical set of PCBs (joint control unit, power inverter unit and power supply unit) and dedicated heaters, as well as an equivalent mechanical and thermal design, so that the same thermal-control concept applies to both sides.

The EB thermal design is driven by two coupled aspects. First, the EBs contain the major share of the arm's internal dissipation in the operational modes due to control electronics and power conversion. Second, the EBs contain temperature-sensitive electronic components that must remain within specified temperature limits in both non-operational and operational conditions, especially in view of the orbit-induced external thermal cycling.

In order to manage the operational dissipation, the thermal design concept uses the EB housings as the main conductive thermal interface. Heat from the PCB assemblies is coupled via a bolted, gap-pad-supported PCB-Housing interface to the aluminium (AA 7075) housings, where it is further distributed into the segement structure. In addition, for mechanical support, the PCB stack is secured with bolted standoffs, which also provide a secondary conductive heat path to the housing. Beyond establishing conductive coupling into the housing, this overall design concept further mitigates the asymmetric operational heat load inherent to cold redundancy, in which only one EB half is powered while the other remains inactive. The segment structures distribute the heat around the full circumference and thereby limit the resulting temperature gradient to only a few K.

Radiative heat rejection is provided by dedicated radiator foils on the external EB housing surfaces. The radiator implementation is described in the next subsection addressing the arm-segment thermal design concept for the external thermal environment.

Compliance with the specified temperature limits in cold conditions is ensured by active thermal control using two dedicated heater per EB half. Due to the dense, double-sided PCB layout and connector placement constraints, direct placement on the surfaces is not feasible. The foils are therefore integrated on the inner side of the internal plate, heating the PCBs mainly through the aluminium housing. Heater power sizing compensates for heat losses through the external EB housing surfaces.

C. Arm Segments

At segment level, joints and EBs are connected through structural links, forming the arm's kinematic chain. The segment thermal design focuses on two aspects: conductive coupling of the electronics dissipation into the structural links and the management of radiative coupling to the external environment via the external surfaces.

The structural links are manufactured from AA 7075 (coated with Surtec 650) and, together with the bolted flange interfaces, provide the dominant conductive heat-transfer paths within each segment. The high thermal conductivity of aluminium, combined with the tubular geometry, enables heat distribution along the link and around the circumference, thereby limiting local hot spots and reducing temperature gradients.

To reduce the sensitivity of the segments to orbit-driven cyclic radiative loads from direct solar, Earth infrared, and albedo fluxes in the LEO environment, a conventional thermal-design approach is applied: the arm is insulated with a 10-layer multi-layer insulation (MLI) blanket wherever feasible. Local tailoring is limited to dedicated radiator areas for heat rejection and kinematic clearances. An overview of the resulting insulation layout is shown in Figure 6.

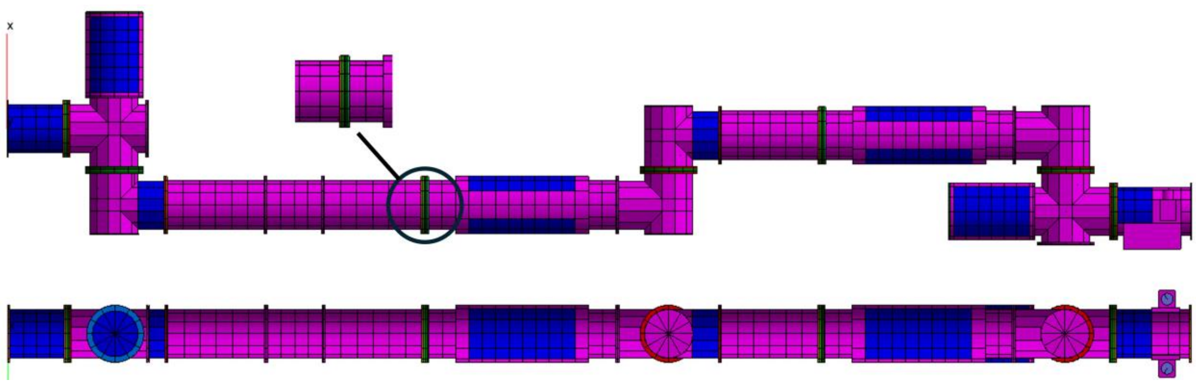

Figure 6. Overview of the arm insulation layout with local tailoring: MLI blanket (magenta), radiator SSM surfaces (blue) and locally uncovered clearance regions at the joints (magnified detail).

For kinematic clearance, the joint interfaces remain uncovered to allow relative motion between the motor and torque sides. Although the Surtec finish on these exposed interfaces has an unfavorable solar absorptivity (up to $\alpha \approx 0.25$), the surface areas are small and the high thermal conductivity of aluminium efficiently spreads the absorbed heat, so no further mitigation is required. Furthermore, the MLI is tailored such that solar trapping at these transition gaps remains negligible.

All radiators are equipped with second-surface mirror (SSM) foils for sun protection. At the EBs, window-shaped cut-outs are made in the MLI blanket on both housing halves to enable controlled heat rejection during operation, since the electronics represent the main operational heat load of the arm. In other local regions where radiating surfaces are needed to mitigate potential hot spots and support temperature homogenisation, the MLI openings are adapted to the local geometry and interface constraints.

Driven by the high configurational flexibility of the robotic arm, radiator view factors are configuration-dependent. In folded configurations, radiator faces near the EBs can oppose each other, reducing their view to deep space and increasing mutual radiative exchange. This effect was accounted for during radiator sizing and verified by analysis, as shown later.

Beyond the conductive and radiative design features described above, the electrical harness is thermally relevant because it interconnects joints and EBs across segment boundaries, introducing parasitic conductive paths along the arm. Depending on routing and interfaces, these paths can support temperature homogenisation or create heat leaks at boundary interfaces (e.g., to the servicer or end-effector). Radiative coupling due to harness exposure is largely eliminated by the hollow-shaft joint design, which allows the cables to be routed entirely internally within the arm.

D. Heating Lines

The CAESAR arm uses a distributed active thermal-control architecture that groups the EBs and joints into four independent heating lines (HL) used for non-operational and operational temperature regulation (see Figure 7).

Each line includes nominal and redundant paths and is referenced to a dedicated temperature control point (TCP) located on the nominal half of the associated EB, instrumented with redundant temperature sensors.

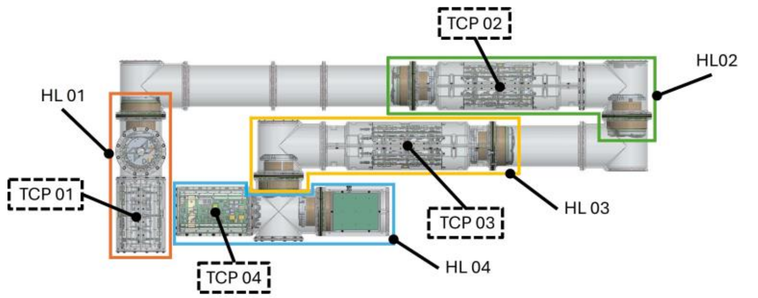

Figure 7. CAESAR arm heating lines (HL01–HL04) and associated temperature control points (TCP01–TCP04) at the EBs.

The applicable arm-level acceptance temperature limits are summarised in Table 2, together with a minimum performance temperature to ensure joint mobility by maintaining sufficiently low friction in the Braycote-lubricated drivetrain. For heater control, these limits were mapped to the EB-located TCP setpoints for each HL, which covers the associated EB and the neighboring joints.

During operation, the temperature limits are additionally monitored using distributed on-board NTC thermistors on the PCB assemblies.

Table 2. CAESAR Arm - Acceptance Temperature Range.

Min. Non-Op.	Min. Op.	Max. Op.	Max. Non-Op	Performance
-35°C	-25°C	+55°C	+65°C	-20°C

In contrast to the segment partitioning, the HL concept does not subdivide a joint into separate control regions. Instead, each assigned joint module (motor and torque side) is controlled as one unit to support homogeneous joint temperature by preventing independent activation and setpoint control of motor and torque side.

In the EROSS SC mission, this heating-line infrastructure is foreseen to be commanded and regulated by the servicer thermal control system (TCS).

VI. Thermal Design Verification

Verification of the CAESAR arm thermal design was performed by using a kinematically configurable subsystem-level ESATAN-TMS model, combined with a simplified servicer representation. The objective was to assess compliance with segment- and component-level temperature limits for a initial set of orbital boundary conditions and arm postures in chasing-mode, covering both non-operational and operational cases. Close-proximity operations were not considered at this stage.

A. Analysis Case Definition

Given the arm's seven-DoF kinematics and the resulting large workspace, the transient thermal analysis was limited to a finite number of postures selected to capture variations in radiative view factors between arm components, the servicer, and the orbital environment as well as configuration-dependent self-shadowing (see Figure 8).

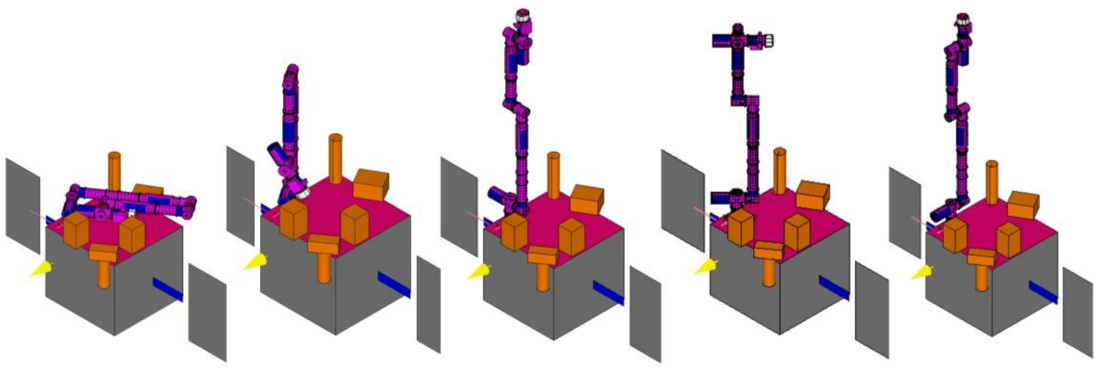

Figure 8. Selected arm postures used for the thermal analysis.

The storage posture represents the launch configuration, in which the arm is stowed compactly close to the servicer platform, with multiple surfaces facing each other. For the non-operational assessment, a safe anti-Sun-pointing attitude of the servicer was assumed in which the platform shades the arm from direct solar irradiation, making this posture a conservative cold-case scenario.

In the folded posture, the arm is oriented such that significant self-viewing occurs across multiple segments, particularly in the radiator regions. Although this configuration is not expected for nominal mission operations, it serves as a conservative sensitivity case, in which self-shadowing reduces the effective view to space and increases mutual radiative exchange within the arm. The effect is most pronounced between Segments 04 and 06 where opposing radiator surfaces mainly view each other, so radiative exchange dominates over heat rejection to space.

For the long posture, the arm is fully deployed, maximising radiative exposure to the orbital environment. Three Joint 01 rotation variants were evaluated (Long-0°, Long-45°, Long-90°). The orientations were established for hot case analyses and selected such that solar incidence on each operational EB half and its radiator is maximized in at least one of the configuration.

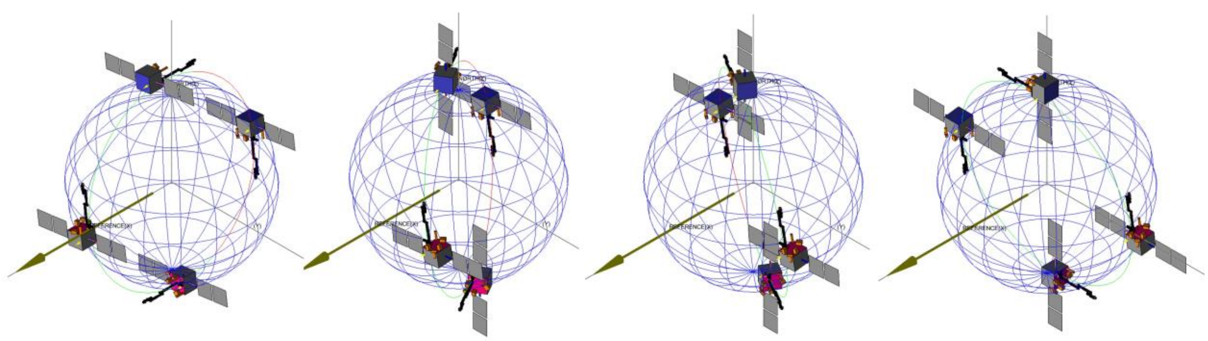

Figure 9. RAAN sampling used for the chasing-mode analysis, shown for the Long-0° arm posture.

To capture the illumination variation across the specified broad RAAN range for the operational cases, a sweep was used to assess the coupled thermal response of orbit-plane orientation and arm posture and to identify sizing-relevant cases. Posture-dependent self-shadowing and changes in solar incidence on the radiators can shift the external heat-loads in a manner that are not obvious from the individual parameters alone. The orbit was therefore discretised by sampling RAAN in 30° increments to provide sufficient angular resolution while keeping the case set compact. Figure 9 illustrates the selected RAAN samples for the analysis, exemplified for the Long-0° arm posture.

For the non-operational cold assessment, the analysis was limited to RAAN = 0° and RAAN = 90°, since these orientations directly capture the longest eclipse phase and continuous minimum external flux condition, respectively, and can therefore directly be identified as the sizing worst cold cases.

Furthermore, one simplification was applied in this analysis: the Sun declination was fixed to 0°, as its impact is captured by the selected cases, which already cover the longest-eclipse and maximum Sun-exposure conditions. Furthermore, its influence across the RAAN range is expected to be minor for the free-flight without close-proximity to a client. This assumption will, however, be validated in future work.

B. Thermal Verification Results

Together, the selected postures and RAAN samples, evaluated for hot- and cold-case boundary conditions, resulted in a total of 30 analysis cases. From this case set, six sizing combinations of orbit orientations and arm postures were identified, as listed in Table 3. Although intermediate RAAN samples (30° and 60°) were included as part of the sweep, they did not result in additional sizing-relevant operational cases. Maximum heater power demands as well as minimum temperature margins occur solely at RAAN = 0° and RAAN = 90°.

Table 3. Overview of sizing orbit orientations and arm postures.

Case	Cold Non-Op.	Cold Non-Op.	Cold Op.	Hot Operational		
Posture	Storage	Storage	Long-90°	Long-45°	Long-90°	Folded
RAAN	0°	90°	0°	90°	90°	90°
Rationale	Longest ecplise phase	Min. env. fluxes	Coldest op. case	Max. Sun exposure for EB 01 and 04	Max. Sun exposure for EB 02 and 03	Min. radiator view-factor to space
Sizing Impact	Peak heater power	Max. average heater power	Seg. 01-04 heating sensitivity	Min. design margin on Seg. 01-03	Min. design margin on Seg. 06 and 08	Design margin self-viewing sensitivity

1. Cold Non-Operational

Figure 10 illustrates the orbital scenario used for the heater-sizing analysis in the storage posture at RAAN = 0° and 90°.

RAAN = 0° drives the peak heater-power demand because the orbit includes flight over the subsolar point, resulting in high environmental fluxes from albedo and Earth, while also featuring the longest eclipse phase. This leads to the steepest cooling rate at eclipse entry.

In contrast, RAAN = 90° results in the highest average heater power demand, as the orientation is characterized by minimal environmental-flux inputs over the full orbit, leading to a continuous heater requirement.

For both non-operational cases, the HL architecture demonstrates robust performance: all electronic components remain within their specified temperature limits, and sufficient heater-power margin is maintained relative to the available budget.

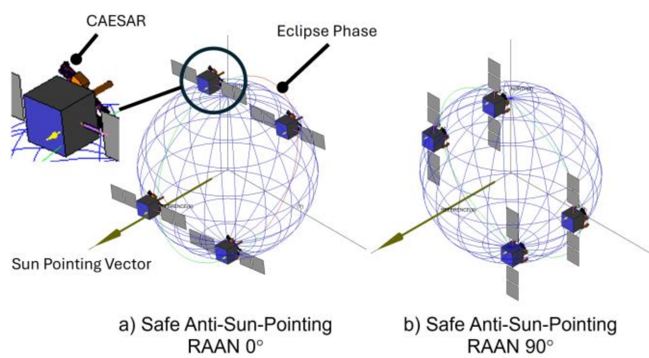

Figure 10. Safe anti-Sun-pointing attitude with CAESAR in the storage configuration for RAAN 0° and RAAN 90°.

2. Cold Operational

In the operational cold case, the Long-90° posture at RAAN = 0° is the sizing combination. The EB power dissipation keeps the arm within the temperature limits without heater activation for most of the orbit. Over a short interval, Segments 01-04 (HL 01 and 02) fall below the operational temperature range. This transient undershoot is primarily driven by a conservative 20% maturity margin applied as a reduction to the EB power dissipation. In the next design phase, this margin will be revisited based on an improved subsystem definition and model correlation, together with a further refinement of the radiator areas. These updates are expected to remove the need for heater activation in cold-case operations. For the remaining Segments 05-08, the average design margin to the predicted compontent temperature limit at Tmin ranges from +1.25 °C to +6.30 °C, confirming sufficient operational compliance.

3. Hot Operational

For the operational hot case, RAAN = 90° is identified as the sizing orientation for all arm configurations. Table 4 summarises the corresponding average segment-level design margins for the Long-45°, Long-90° and Folded postures and indicates the posture-dependent limiting segments.

Table 4. Average segment-level design margins at Tmax (operational hot case, RAAN = 90°).

Segment	EB	Long-45°	Long-90°	Folded
Segment 01	-	+6.36 °C	+10.10 °C	+4.98 °C
Segment 02	EB 01	+5.83 °C	+15.02 °C	+0.99 °C
Segment 03	-	+9.82 °C	+17.38 °C	+7.08 °C
Segment 04	EB 02	+13.72 °C	+15.46 °C	+6.62 °C
Segment 05	-	+14.84 °C	+15.46 °C	+5.49 °C
Segment 06	EB 03	+15.45 °C	+12.85 °C	+2.79 °C
Segment 07	EB 04	+12.59 °C	+15.40 °C	+2.15 °C
Segment 08	-	+14.71 °C	+3.48 °C	+0.21 °C

Among the analysed long postures, Long-45° shows the lowest design margins on Segments 01-03, which is consistent with the EB 01 radiator areas being maximally exposed to the Sun. A similar sun-orientation effect also occurs on Segment 07 through the EB04 radiator areas, but the impact on the design margin is less pronounced. The reason is that, in the deployed arm configuration, Segment 07 maintains a clear view to deep space, whereas Segments 01-03 are additionally influenced by the servicer surroundings. As a result, radiator heat rejection is higher on Segment 07, limiting the margin reduction. The remaining segments maintain higher margins, confirming robust hot-case compliance.

In contrast, for Long-90° the lowest average design margins can be found on Segments 06 and 08, with the minimum at Segment 08. In this posture, although the orientation has been primarily selected for the radiators of EB 02-03 (Segments 04 and 06, respectively), the Segment 08 radiator is also facing the Sun. Since it is single-sided (see Figure 11), the opposite side provides no surface for heat rejection, which increases sensitivity to solar exposure and results in higher temperatures. By comparison, Segment 06 shows a less pronounced design margin reduction because the effectiveness of the EB 03 radiator concept is supported by additional surface area on the opposite side.

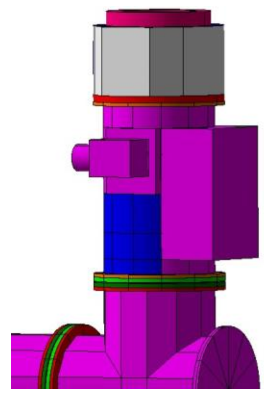

Figure 11. Single-sided radiator (blue) of Seg. 08.

A further outcome of the analysis case is that Segment 04 does not show a comparable margin reduction to Segment 06, despite the two segments being similar in design and EB 02 having the same sun-oriented radiator exposure. This can mainly be explained by the asymmetric neighboring geometry: Segment 03 is longer than Segment 05, which improves heat spreading and temperature homogenisation.

Across the remaining segments, Long-90° exhibit higher margins than Long-45°. This highlights how even small arm rotations can change the thermal behaviour, with individual segments responding differently under the same hot-case orbital environment.

Finally, the folded posture, as a conservative configuration, results in the smallest overall segment-level design margins. Due to self-viewing of CAESAR, the values drop significantly compared to the long postures for the whole arm. While compliance is still maintained, the reduction demonstrates that folded, self-blocking geometries are particularly sensitive and should be prioritised in follow-on analyses, especially under close-proximity conditions.

VII. Conclusion and Future Work

This paper presented the thermal design of the CAESAR seven-DoF robotic arm for the EROSS SC mission context and the modelling approach to perform a first thermal verification for the free-flight chasing mode.

The thermal concept addresses the modular architecture of the distributed joint modules and EBs by applying dedicated thermal design measures to each unit. At segment level, extensive MLI insulation is used to limit the impact of orbit-driven thermal loads and is complemented by dedicated radiator areas on the EBs and selected surfaces to provide controlled heat rejection and support a more uniform temperature distribution along the arm. Active cold-case temperature control is realized via heaters arranged in four heating lines.

A kinematically configurable subsystem-level ESATAN-TMS model of the arm, combined with a simplified servicer representation, was used to perform the chasing-mode verification against segment- and component-level temperature limits. The verification covered selected arm postures and orbit-to-Sun geometries, resulting in 30 analysis cases and six sizing combinations. The segment-level results show that, in the non-operational cold cases, the heating-line architecture maintained the EB-referenced TCPs within limits with sufficient margin to the servicer power budget. Compliance was also maintained for the assessed operational hot and cold environments. However, design margins depend strongly on arm posture, and self-shadowing configurations are particularly sensitive due to reduced heat rejection. During the RAAN sweep from 0° to 90° in 30° increments, the intermediate orientations did not introduce additional sizing conditions. This observation applies to the assessed cases but may differ for close-proximity operations where additional servicer–client radiative coupling becomes relevant.

Overall, the verification results confirm that the presented thermal design and control concept provides robust compliance across the assessed chasing-mode envelope. The described modelling approach is not limited to CAESAR and can be applied to other articulated servicing arms to identify posture-dependent worst-case thermal scenarios.

As next step, the verification scope will be extended to close-proximity operations, where radiative coupling and shadowing between the servicer, the arm, and the client are expected to become dominant drivers of the thermal boundary conditions. These conditions will be assessed using a coupled geometric representation of the RAS to capture mutual radiative exchange and configuration-dependent view factors, including end-effector hardware such as the HOTDOCK interface and the LARIS gripper as additional exchange partners.

With the introduction of close-proximity parameters and additional mission-level variables, case selection becomes more complex and configuration-dependent. Identifying a bounding set of sizing cases that balances coverage of the mission envelope with verification effort will become a key task. This provides the basis for robust subsystem-level thermal-control solutions and deriving operational constraints and mitigation strategies (e.g., maximising operational flexibility, minimising heater-power demand, and selecting thermally favorable arm postures).

In order to support this process, follow-on work will focus on the development of an analysis tool to systematically screen and verify sizing cases and to quantify configuration sensitivities. The tool will parametrise the arm kinematics together with key mission variables, including orbit altitude, orbit-to-Sun geometry (including Sun declination), proximity distance and relative orientation, as well as mission-relevant attitudes and operational modes. Where operational mitigation is required, the tool could evaluate null-space self-motion manoeuvres that maintain the required end-effector pose while shifting joint angles towards thermally favorable configurations. Beyond sizing, the tool could also support mission maturation and operations planning by analysing and comparing approach, capture, and ORU-transfer operation scenarios from a thermal perspective.

Furthermore, verification and model correlation will be extended beyond joint level through segment-level thermal testing. The outcomes of this work will feed back into the overall thermal analysis and support fine-tuning of the thermal design, for example by refining radiator sizing and layout, MLI tailoring, and heater-control settings.

Acknowledgments

The authors gratefully thank the CAESAR team for their contributions to the development and the EROSS team, as well as the external reviewers, for very valuable discussions.

Disclaimer

Funded by the European Union. Views and opinions expressed are however those of the author(s) only and do not necessarily reflect those of the European Union or European Health and Digital Executive Agency (HaDEA). Neither the European Union nor the granting authority can be held responsible for them.

References

[1] A. S. Jones, A. M. Gray and A. Kong, "The Thermal Design, Analysis and Testing of the Shuttle Remote Manipulator Arm," in *14th AIAA Thermophysics Conference*, Florida, USA, 1979.

[2] R. Kumar and R. Hayes, "System Requirements and Design Features of Space Station Remote Manipulator System Mechanisms," in *25th Aerospace Mechanisms Symposium*, Pasadena, USA, 1991.

[3] Y. Boillot and G. I. M. Beere, "Thermal Control Design of the European Robotic Arm (ERA)," in *6th European Symposium on Space Environmental Control Systems*, Noordwijk, The Netherlands, 1997.

[4] A. Beyer, G. Grunwald, et al., "CAESAR: Space Robotics Technology for Assembly, Maintenance, and Repair," in *69th International Astronautical Congress (IAC)*, Bremen, Germany, 2018.

[5] G. Hirzinger, K. Landzettel, et al., "ROKVISS - Robotics Component Verification on ISS," in *8th International Symposium on Artificial Intelligence, Robotics and Automation in Space (iSAIRAS)*, Munich, Germany, 2005.

[6] EROSS SC, "What is EROSS SC - Our mission and values," [Online]. Available: https://www.eross-sc.eu/about/what-is-eross-sc/. [Accessed 14 February 2026].

[7] EROSS SC, "Partners," [Online]. Available: https://www.eross-sc.eu/about/partners/. [Accessed 14 February 2026].

[8] M. A. Roa, A. Beyer, et al., "EROSS: In-Orbit Demonstration of European Robotic Orbital Support Services," in *IEEE Aerospace Conference (AERO)*, Big Sky, USA, 2024.

[9] P. Letier, T. Siedel, et al., "HOTDOCK: Evolution Towards a Space Qualified Standard Interface for In-Space Operations and Servicing Applications," in *75th International Astronautical Congress (IAC)*, Milan, Italy, 2024.

[10] Ł. Kozłowski, A. Łukasiak, et al., "Design and Development of a Robotic Gripper for Capturing Prepared and Unprepared Satellites," in *20th European Space Mechanisms and Tribology Symposium (ESMATS)*, Warsaw, Poland, 2023.